Journal of Alloys and Compounds 526 (2012) 103–109

Contents lists available at SciVerse ScienceDirect

Journal of Alloys and Compounds

journal homepage: www.elsevier.com/locate/jallcom

Effects of AlN nucleation layers on the growth of AlN films using high temperature hydride vapor phase epitaxy

M. Balaji[a,b,c], A. Claudel[b], V. Fellmann[a], I. Gélard[b], E. Blanquet[a,*], R. Boichot[a], A. Pierret[d,e], B. Attal-Trétout[d], A. Crisci[a,f], S. Coindeau[a,f], H. Roussel[f], D. Pique[b], K. Baskar[c], M. Pons[a]

[a] Science et Ingénierie des Matériaux et des Procédés, Grenoble INP-CNRS-UJF, BP 75, 38402 Saint Martin d'Hères, France
[b] ACERDE, 452 rue des sources, 38920 Crolles, France
[c] Crystal Growth Centre, Anna University-Chennai, Chennai 600025, India
[d] Département de Mesures Physiques, ONERA, Chemin de la Hunière, 91761 Palaiseau Cedex, France
[e] CEA-CNRS Group "NanoPhysique et SemiConducteurs", INAC/SP2M/NPSC, CEA-Grenoble, 17 rue des Martyrs, 38054 Grenoble, Cedex 9, France
[f] CMTC, Grenoble INP, 38402 Saint Martin d'Hères, France

ARTICLE INFO

Article history:
Received 25 November 2011
Received in revised form 14 February 2012
Accepted 17 February 2012
Available online xxx

PACS:
68.55.A–
68.55.–a
68.55.J–
61.05.cp
81.15.Gh
81.05.Ea

Keywords:
Nucleation
X-ray diffraction
High temperature hydride vapor phase epitaxy
HT-HVPE
Nitrides
AlN
Semiconducting aluminum compounds

ABSTRACT

AlN layers were grown on *c*-plane sapphire substrates with AlN nucleation layers (NLs) using high temperature hydride vapor phase epitaxy (HT-HVPE). Insertion of low temperature NLs, as those typically used in MOVPE process, prior to the high temperature AlN (HT-AlN) layers has been investigated. The NLs surface morphology was studied by atomic force microscopy (AFM) and NLs thickness was measured by X-ray reflectivity. Increasing nucleation layer deposition temperature from 650 to 850 °C has been found to promote the growth of c-oriented epitaxial HT-AlN layers instead of polycrystalline layers. The growth of polycrystalline layers has been related to the formation of dis-oriented crystallites. The density of such disoriented crystallites has been found to decrease while increasing NLs deposition temperature. The HT-AlN layers have been characterized by X-ray diffraction $\theta - 2\theta$ scan and (0 0 0 2) rocking curve measurement, Raman and photoluminescence spectroscopies, AFM and field emission scanning electron microscopy. Increasing the growth temperature of HT-AlN layers from 1200 to 1400 °C using a NL grown at 850 °C improves the structural quality as well as the surface morphology. As a matter of fact, full-width at half-maximum (FWHM) of 0 0 0 2 reflections was improved from 1900 to 864 arcsec for 1200 °C and 1400 °C, respectively. Related RMS roughness also found to decrease from 10 to 5.6 nm.

1. Introduction

Aluminum nitride (AlN) single crystal is a promising substrate material for AlGaN based ultraviolet light emitting diodes (UV LEDs) [1], piezoelectric sensors [2], high-power and high temperature electronic devices [3,4] owing to its wide band gap (6.2 eV), high thermal conductivity (3.2 W cm^{-1} K^{-1}) and excellent lattice match with gallium nitride (GaN) [5,6]. AlN bulk single crystals grown by sublimation-recondensation and solution growth methods [7–10] are still limited by the size. Several techniques for growing aluminum nitride layers on a variety of substrates have been used, including molecular beam epitaxy (MBE) [11], metal-organic vapor phase epitaxy (MOVPE) [12] and hydride vapor phase epitaxy (HVPE) [13]. However thick AlN layers grown using HVPE or High Temperature Halide Chemical Vapor Deposition (HTCVD) [14] on sapphire (Al_2O_3) substrates have been widely considered as the alternative for the production of AlN substrates [15], due to the low cost and availability of Al_2O_3 in larger diameter. The large lattice mismatch between AlN and sapphire as well as poor Al adatom migration [12] makes high quality AlN growth on sapphire substrate more difficult than GaN neither by MOVPE nor by MBE. The initial growth stage plays a very important role in GaN and AlN epitaxial growth. The GaN epilayers with low-temperature AlN nucleation layers (NLs) have been vastly studied when compared to AlN epilayers grown on low temperature AlN NLs [16]. To achieve high growth rate, good surface morphology and crystalline quality,

* Corresponding author. Tel.: +33 04 76 82 66 49; fax: +33 04 76 82 66 77.
E-mail address: elisabeth.blanquet@simap.grenoble-inp.fr (E. Blanquet).

0925-8388/$ – see front matter © 2012 Elsevier B.V. All rights reserved.
doi:10.1016/j.jallcom.2012.02.111

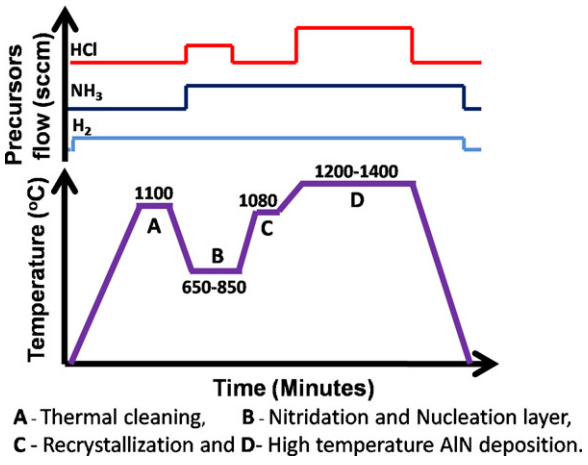

Fig. 1. HT-AlN Process temperatures and precursors flow *vs* time.

AlN deposition requires a high growth temperature above 1200 °C [14,17]. Nevertheless, thermal decomposition of c-plane sapphire starts to occur at 1200 °C [18] and AlN starts to decompose around 1400 °C [19] by reacting with hydrogen (H_2) used as a carrier gas, resulting in the formation of surface pits and in the degradation of AlN layer quality [20].

In this paper, the potential effect of using low temperature NLs for the growth of AlN layers by high temperature hydride vapor phase epitaxy (HT-HVPE) has been examined. The main idea is to grow AlN NLs at temperatures typically used in the case of AlN epitaxial growth by MOVPE [21,22] and higher than those used in the case of GaN epitaxial growth by MOVPE [23,24]. The significance of low temperature AlN NLs as well as deposition temperature of HT-AlN layers and its effects on surface morphology, structural and optical quality of AlN layers have been investigated.

2. Experimental procedure

AlN films were grown using HT-HVPE. The HT-HVPE setup consists of graphite susceptor heated by induction in a vertical water-cooled cold-wall reactor. The growth temperature was measured using a thermocouple inserted into the graphite susceptor [25]. Aluminium chloride ($AlCl_3$) and ammonia (NH_3) were used as the precursors for AlN deposition. $AlCl_3$ was formed through the *in situ* reaction between aluminium (Al) pellets and hydrogen chloride (HCl_g) at 500 °C. Hydrogen (H_2) was used as carrier gas. All the precursors used were 5 N (99.999%) grade purity. AlN growths were performed on 2″ c-plane sapphire epi-ready wafers. Sapphire substrate was loaded on graphite susceptor and thermally cleaned at 1100 °C for 10 min under H_2 ambient. Thermal cleaning was followed by nitridation, deposition of nucleation layers, recrystallization of NLs and growth of HT-AlN films.

To improve the quality of HT-AlN films, the NLs have been examined by varying deposition temperatures. The nucleation layer was deposited at 650, 750 and 850 °C on c-plane sapphire substrates. The as-grown NLs were first characterized then the same samples were reloaded into the reactor to perform high temperature (HT)-treatment. In order to study the characteristics of NLs prior to HT growth (without growing HT-AlN layers), the NLs were recrystallized at 1080 °C and further ramped up to 1200 °C (high temperature treatment) then cooled down under $H_2 + NH_3$ ambient. The NLs V/III flux ratio was kept constant at 30. The V/III ratio in the gas phase is calculated as the $NH_3/AlCl_3$ inlet flow rates ratio assuming that the chlorination reaction yield is equal to 1 and that $AlCl_3$ is the predominant $AlCl_x$ species [26]. The NLs were overgrown for 60 min to deposit high temperature (HT)-AlN layers. HT-AlN layers have been grown at 1200 °C directly on AlN nucleation layers after HT treatment (without air exposure). HT-AlN layers were grown in three groups, classified by the variation in nucleation layer deposition temperatures 650, 750 and 850 °C. Four HT-AlN samples have been grown in each NL deposition temperatures (650, 750 and 850 °C), all the 12 samples were grown with a V/III ratio of 10. Throughout all the growth steps, 2200 sccm of H_2 flow and 100 sccm of NH_3 flow were used and reactor pressure was maintained at 10 mbar (1300 Pa). Fig. 1 shows the growth steps of the HT-AlN layers.

The grown HT-AlN films with NLs deposited at different temperatures were structurally characterized by X-ray diffraction (XRD) using $\theta - 2\theta$ scan, rocking curve (XRC) of the (0 0 0 2) peak, Raman and photoluminescence (PL) spectroscopies. PL measurements were performed at low temperature (5 K) using an ArF-excimer laser emitting at 193 nm (6.42 eV). Surface morphology was accessed by tapping mode atomic force microscopy (AFM) and field emission scanning electron microscopy (FE-SEM). The RMS roughness was measured on 1 μm × 1 μm scan for NLs and 5 μm × 5 μm scan for HT-AlN samples. The average thickness of NLs and HT-AlN samples was measured by X-ray reflectivity (XRR) and cross sectional FE-SEM respectively. The thickness of all the HT-AlN samples was found to be approximately 2 μm. Finally, a comparison was made between the quality of HT-AlN films grown at 1200 and 1400 °C by employing optimal NLs process parameters.

3. Results and discussion

3.1. Low temperature nucleation layers

3.1.1. Surface morphology

The variation in surface morphology of NLs with respect to the deposition temperature is presented in Fig. 2. Fig. 2a and c shows the surface morphology of as-grown NLs at 650 and 850 °C. Fig. 2b and d depict the surface morphology of HT-treated NLs grown at 650 and 850 °C. The RMS roughness values for as-grown NLs at 650 °C (Fig. 2a) and HT-treated NLs (Fig. 2b) are found to be 3.5 nm and 2.5 nm respectively. The RMS roughness for as-grown NLs at 850 °C (Fig. 2c) and HT-treated NLs (Fig. 2d) are 1.3 nm and 1.0 nm, respectively. It is found that the RMS roughness decreases after HT-treatment, which is contradicting to AlN NLs grown using MOVPE [27]. The reduction in the RMS roughness values after the HT-treatment can be attributed to the rearrangement of nucleation islands (NIs) height. On the investigated surface under both deposition temperatures, the size of the NIs is found to vary and it can be distributed as small (<35 nm diameter and <4 nm height) and relatively big islands (>40 nm diameter and >5 nm height).

Table 1 presents the NIs density, size and height observed from the AFM images (Fig. 2). The nucleation islands density for all the nucleation layers is found to be in the order of 10^{11} cm^{-2}. It is worth noting that the difference between small and big NIs densities is more pronounced at 850 °C. At both 650 and 850 °C, the increase of density for big NIs seems to explain the re-distribution process of NIs at high temperatures. However, lowest density of bigger NIs after HT-treatment has been observed at 850 °C NLs when compared with 650 °C NLs. There is almost no change in big NIs diameters after HT-treatment for 650 °C NLs. On other hand, noticeable increase has been observed in NIs diameter after HT-treatment for 850 °C NLs. The NIs height is decreased for both distributions after the HT-treatment of NLs grown at 650 °C whereas the height of both NIs distributions is found to remain unchanged for NLs grown at 850 °C.

Table 1
Nucleation islands (NIs) density, size and height observed from AFM images (Fig. 2).

NL deposition temperature (°C)	Conditions	NI density (10^{10} cm^{-2})		NI diameter (nm)		NI height (nm)	
		Small	Big	Small	Big	Small	Big
650 (Fig. 2a)	As-grown	9	1	15–20	55–65	2–4	10–18
650 (Fig. 2b)	HT-treated	9	6	25–35	50–70	1–3	5–6
850 (Fig. 2c)	As-grown	8	0.08	15–21	40–45	2–3	5–9
850 (Fig. 2d)	HT-treated	10	0.2	20–30	50–75	2–4	5–9

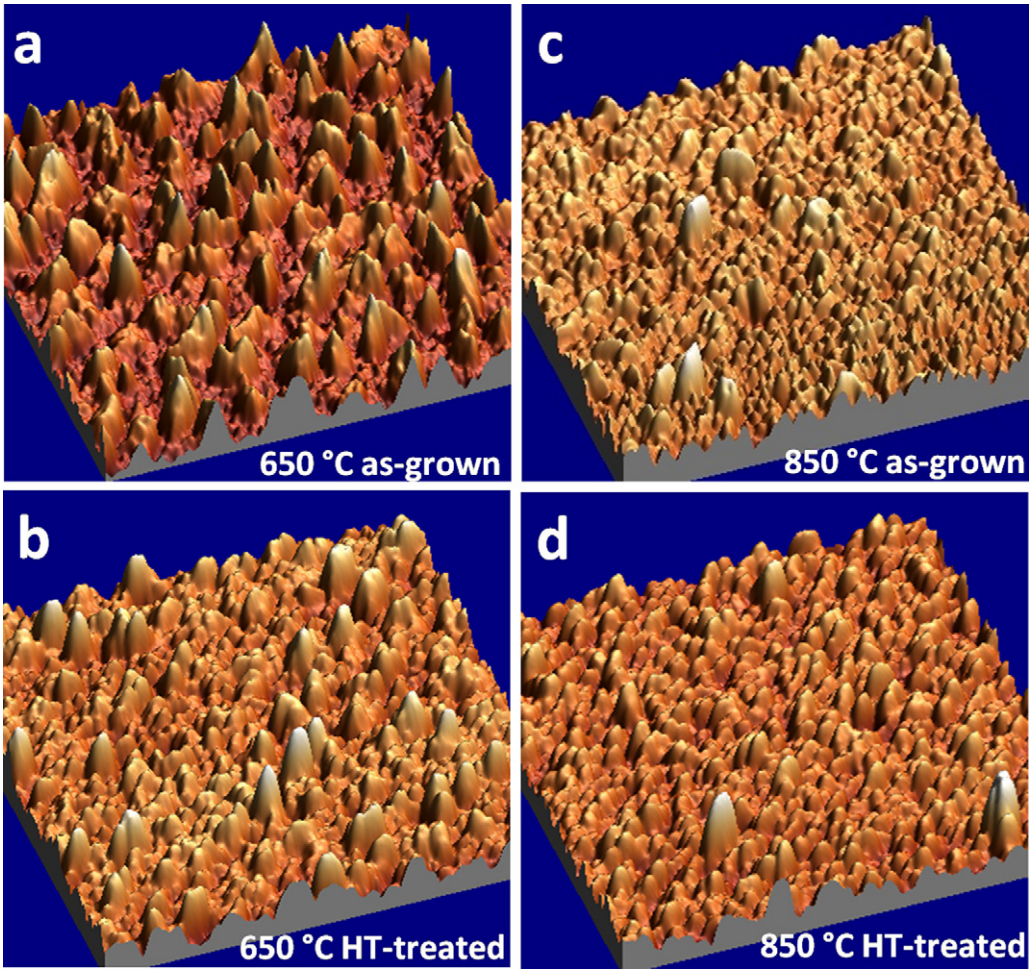

Fig. 2. AFM images of nucleation layer grown at 650 °C (a) as-grown, (b) HT-treated and NL grown at 850 °C (c) as-grown, (d) HT-treated. All images are 1 μm × 1 μm.

3.1.2. Thickness

The thickness of as-grown NLs has been measured by XRR as 8, 11 and 75 nm for samples grown at 650, 750 and 850 °C respectively. The thickness of NLs increases while increasing the NLs deposition temperature from 650 to 850 °C. This is attributed to the faster gas phase diffusion and surface diffusion while increasing the temperature [28]. After HT-treatment the thickness of NLs has been found as 6, 8 and 44 nm for NLs grown at 650, 750 and 850 °C respectively. XRR results show obvious decrease in thickness of the NLs after the HT-treatment. Fig. 3 shows the XRR plot of as grown and HT-treated NLs grown at 850 °C.

There is an obvious reduction in thickness of the NLs deposited at 850 °C after the HT-treatment. This observation shows that AlN NLs may undergo decomposition at lower temperature than 1200 °C, despite the fact that AlN NLs normally do not decompose after annealing at 1030 °C [27]. Changes on surface morphology, re-distribution of NI's density, size and height are observed after the HT-treatment could also explain a part of the thickness reduction. In fact, a too thin or too thick AlN buffer layer will lead to a deteriorated quality of AlN films [29]. The thickness of NLs before HT-AlN layers growth will definitely have an important impact on the HT-AlN layer quality. So, it is expected that the adequate thickness of NLs as well as the largest grain size and the lowest NIs density improves the quality of HT-AlN layers.

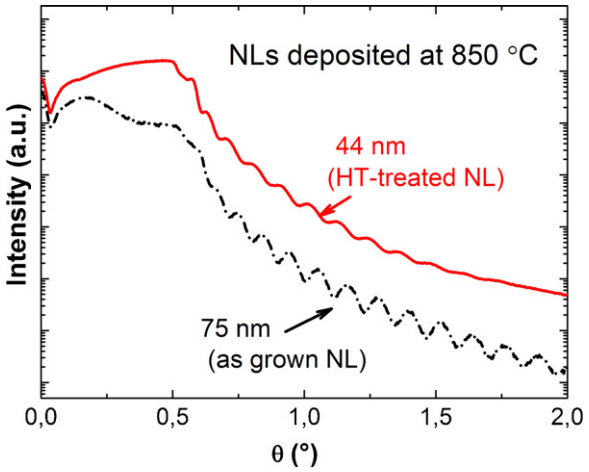

Fig. 3. X-ray reflectivity plot of HT-treated and as grown NLs deposited at 850 °C. The intensity is in a log scale.

3.2. HT-AlN layers using AlN NLs

3.2.1. X-ray diffraction and surface morphology studies

All the HT-AlN samples grown using the NL deposition temperature of 650 °C are polycrystalline and show a $(10\bar{1}1)$ semi-polar

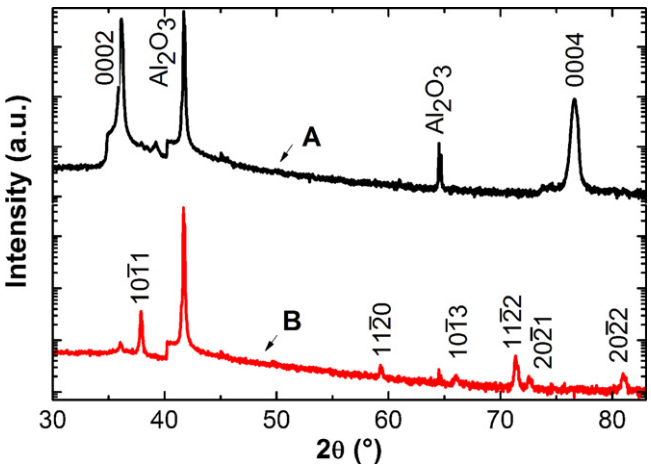

Fig. 4. XRD $\theta-2\theta$ scans of a (0002) oriented HT-AlN layer grown on 850 °C NL (A) and polycrystalline HT-AlN layer with a (10$\bar{1}$1) preferred orientation grown on 650 °C NL (B). The intensity is in a log scale.

predominant orientation. In contrast, most of the HT-AlN samples grown on 750 and 850 °C NLs reveal only a (0002) orientation in $\theta-2\theta$ XRD scans. Fig. 4 shows $\theta-2\theta$ XRD scans of a (0002) oriented HT-AlN layer grown on 850 °C NL (A) and a HT-AlN polycrystalline layer with a 10$\bar{1}$1 preferred orientation grown on 650 °C NL (B). It is important to note that direct growth (without NLs) of AlN films at 1200 °C on sapphire c-plane substrates with the same experimental conditions leading to the growth of semi-polar oriented polycrystalline AlN layers as already observed in the previous work at high growth rate [30]. The introduction of NLs prior to HT-AlN films for wetting the substrate surface, producing the nucleation sites and acting as a buffer layer to accommodate the lattice mismatch between sapphire and AlN films certainly promote AlN epitaxial growth on sapphire.

Fig. 5 depicts the plot between RMS roughness values of HT-AlN layers with the samples predominant orientations as a function of NLs temperatures. The AFM images shown in Fig. 5 disclose HT-AlN sample surface with the lowest RMS roughness values in each group classified with NLs deposition temperatures of 650, 750 and 850 °C, respectively. The surface morphology of HT-AlN layers becomes smoother while increasing NLs deposition temperature. The HT-AlN layers grown with 650 °C NLs favour the semi-polar (10$\bar{1}$1) orientation with polycrystalline morphology. The HT-AlN layers grown with 750 °C NLs show hexagonal pyramid-like features, whereas broad hexagonal pyramids with low step size have been seen at HT-AlN layers grown with 850 °C NLs. Several c-oriented samples surfaces exhibited some encrusted AlN disoriented crystallites. A correlation between surface roughness and the HT-AlN layers preferred orientation has been observed. The polycrystalline layers with (10$\bar{1}$1) preferred orientation exhibit RMS roughness as high as 87 nm whereas epitaxial HT-AlN layers show RMS roughness as low as 10 nm.

XRC measurements have been performed on the (0002) AlN peak in order to determine the crystalline quality of HT-AlN layers exhibiting only the (0002) orientation. It has been found that HT-AlN samples grown with 850 °C NLs disclose narrower (0002) FWHM values than those grown with 750 °C NLs. (0002) FWHM values are 3100 and 1900 arcsec for HT-AlN layers with NLs grown at 750 and 850 °C, respectively. High FWHM are related to high threading dislocation (TD) density, which is highly detrimental to AlN electrical and optical properties [31]. Depending on their Burger vector, TDs could be edge-type, screw-type or mixed-type. The broadening of symmetric (0002) reflection (tilt) and asymmetric reflection (twist) are related to mixed or screw-type dislocations density, and edge-type dislocations density respectively. In the case of randomly distributed dislocations, the TD density D can

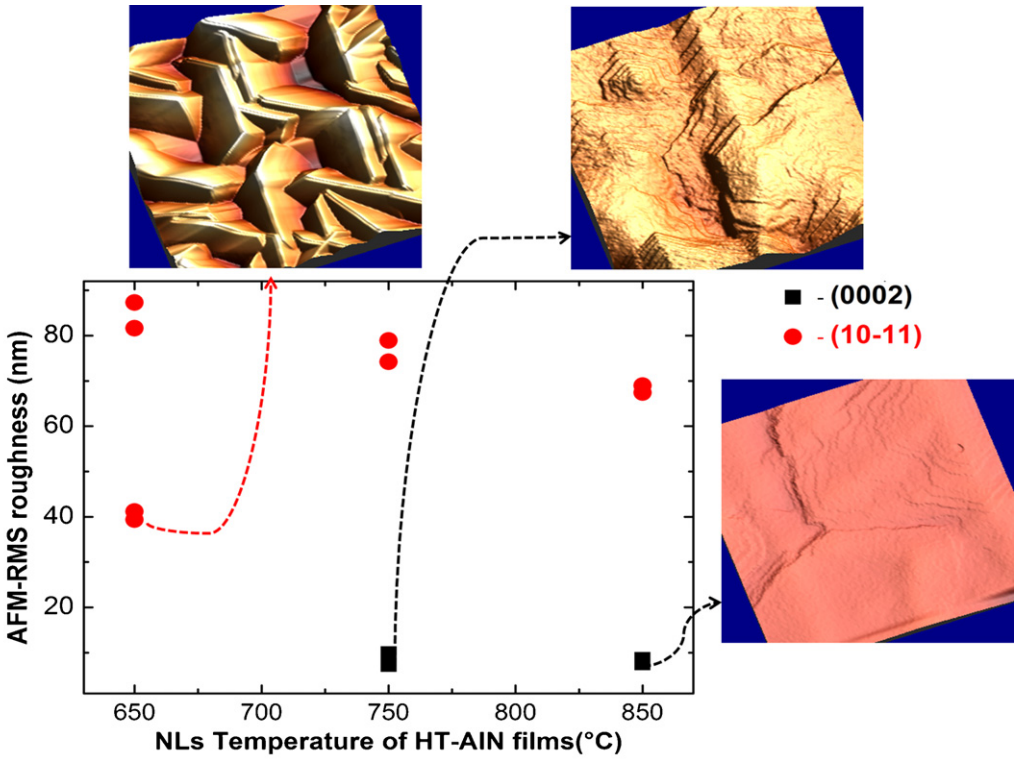

Fig. 5. AFM RMS roughness values of HT-AlN layers against the NLs temperature of HT-AlN layers with samples predominant orientations, (0002) – black squares and (10$\bar{1}$1) – red circles. Corresponding AFM images of the samples with the lowest RMS value in each group are also shown. All AFM images are 5 μm × 5 μm. (For interpretation of the references to color in this figure legend, the reader is referred to the web version of the article.)

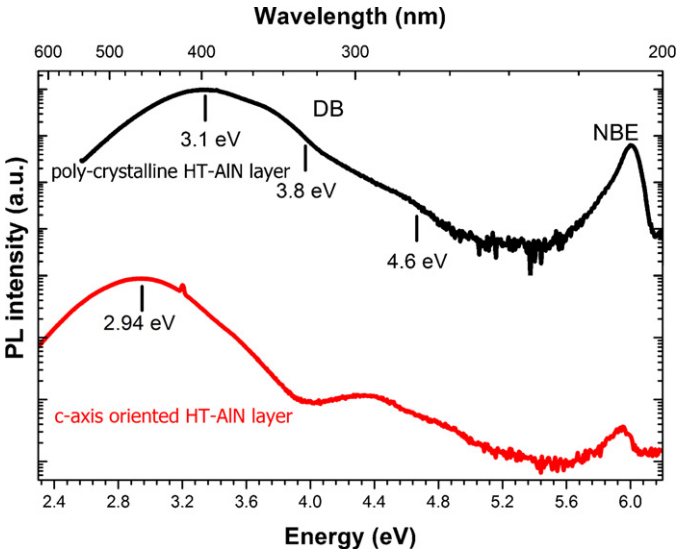

Fig. 6. PL spectra at 5 K for polycrystalline HT-AlN layers with NL grown at 650 °C and *c*-axis oriented HT-AlN layer with NL grown at 750 °C. NBE excitonic emission around 6 eV and several DB related to deep level around 3.1, 3.8 and 4.6 eV.

be roughly estimated from $D = \mathrm{FWHM}^2/4.35b^2$ [32], where FWHM is the peak width of the rocking curve reflection (in radians) and b the Burger vector length. Using the burger vector value of AlN (b_{screw} = 4.982 Å), TD dislocations densities are estimated to be 2×10^{10} and 8×10^9 cm^{-2} for screw-type dislocations in HT-AlN layers grown using 750 and 850 °C NL, respectively.

3.2.2. Photoluminescence measurements

Optical properties are closely related to TD dislocation density. PL measurements at low temperature (5 K) have thus been performed on polycrystalline HT-AlN layers with semi-polar orientation grown on 650 °C NL and *c*-axis oriented HT-AlN layers grown on 750 °C NL shown in Fig. 6. Both layers show single peak near band edge (NBE) emission and additional broad defect bands (DB). Semi-polar oriented polycrystalline layer has NBE emission at 5.99 eV whereas c-oriented layer emits at 5.95 eV. These values are found similar to previous reported ones for HT-AlN layers grown by HT-HVPE (5.95 eV at 300 K, 6.03 eV at 5 K) [33]. The variation of NBE peak position could be assigned to different stress states. The NBE emission has been tentatively assigned to donor bound excitons (D^0X) and DB at 3–4.6 eV to Donor Acceptor Pair (DAP) recombinations. Both layers show defect band related to deep levels located around 3 eV. The c-oriented layer also shows a low intensity band at 4.3–4.9 eV. Probable origin for defect emission is $V_{Al}(O_N)_x$ complexes formed from Al-vacancy and O impurities, the former has been assigned to 4.6 eV band and the later has been attributed for 3 eV DBs [34,35]. The intensities ratio between NBE and DB (at 3 eV) is 0.06 and 0.003 for polycrystalline and *c*-axis oriented HT-AlN layers, respectively. Such ratios indicate incorporation of huge impurities in both layers. It is related to O incorporation inside the HT-AlN layer and could be due to sapphire decomposition followed by O diffusion at high growth temperature. Peak shift position for broad defect band for c-oriented HT-AlN layers towards lower energy could be also attributed to higher O incorporation. The low intensity of NBE emission has also been related to high dislocation densities. The intensity for NBE emission is found 15-folds lower for the c-oriented layer compared to the polycrystalline one, indicating a lower density of O or Si impurities which acts as a shallow donor. Consequently, one possible way to improve the optical properties of the HT-AlN layers is to decrease the TD density (*e.g.* using higher growth temperature for AlN layers) and to decrease O incorporation. Probably the source of such impurities could be the materials present in the reactor like quartz, stainless steel and graphite.

3.2.3. Raman spectroscopy analysis

As several c-oriented samples exhibited some encrusted AlN disoriented crystallites, the crystallographic orientations of such AlN crystallites have been investigated by Raman spectroscopy. Fig. 7a shows Raman spectra performed on c-axis oriented

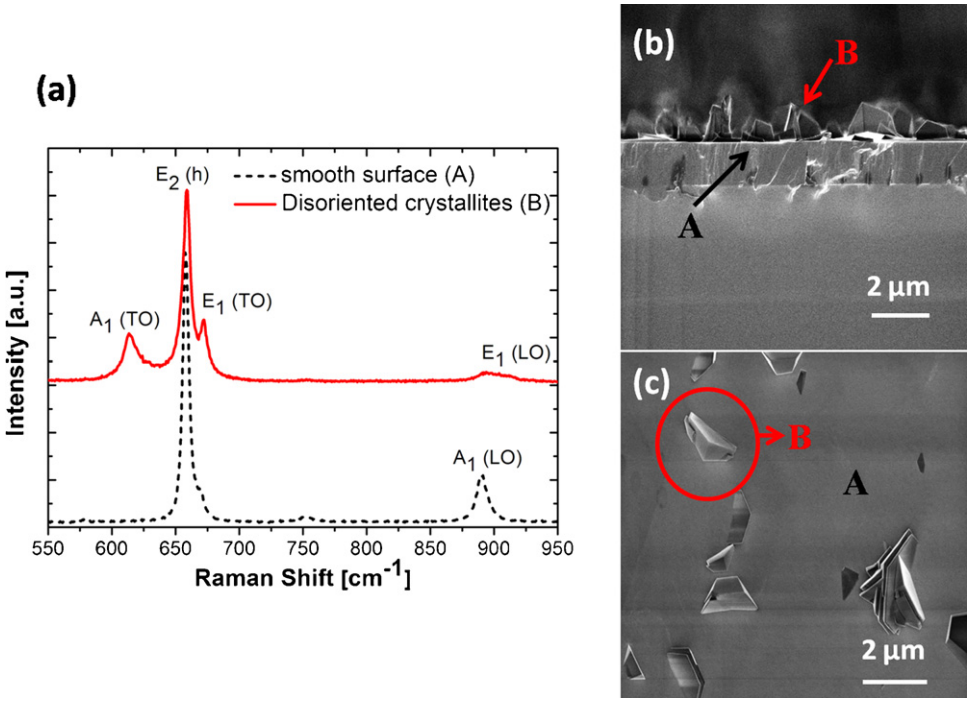

Fig. 7. (a) Raman spectra on c-axis AlN (smooth surface A) and disoriented crystallites (B) of the same sample with NL grown at 750 °C. (b) FE-SEM cross sectional and (c) surface image of AlN showing the c-axis oriented layer (A) and the disoriented crystallites of AlN (B).

surface (denoted as A) and on one disoriented crystallite (denoted as B) of the HT-AlN sample with 750 °C NL. Raman spectra have been recorded using the 514 nm line of an Ar+ ion laser, at room temperature (RT) in a backscattering geometry. All measurements have been made at normal incidence, respective to the sample surface. For this particular geometry, the allowed Raman modes for c-oriented AlN wurtzite structure are non-polar E_2 modes and the polar A_1(LO) mode. The unstrained phonon frequency at room temperature (RT) for AlN are 657 cm^{-1} for the E_2(h) mode and 890 cm^{-1} for the A_1(LO) mode. The frequency of the E_2(h) phonon mode (658 cm^{-1}) for the smooth surface is thus related to limited in-plane compressive strain. As a matter of fact, the crystallites with hexagonal geometry observed on AlN surface having semi-polar orientation (as deduced from $\theta/2\theta$ XRD scans shown in Fig. 4) could exhibit other active modes such as the E_1 modes at 671 cm^{-1} and 912 cm^{-1} for TO and LO modes respectively [36]. It has also been confirmed from Raman phonon modes coming from the disoriented crystallites (facets) with respect to the sample surface. Porto notation is often used to describe the Raman selection rules [37,38]. The *z* direction is along the *c*-axis, *x* and *y* are orthogonal and lie in the substrate plane. Restricting ourselves to the cases where the out coming light follows the incoming excitation light path, only the E_2 and A_1(LO) modes are allowed for the $z(yy)\bar{z}$ scattering configuration, whereas the A_1(TO) mode is allowed for $y(zz)\bar{y}$ and $y(xx)\bar{y}$ configuration. E_1(TO) phonons mode is Raman active for $y(xx)\bar{y}$ scattering geometry. It is worth noticing that TO modes are only allowed when 90° configuration is used (excitation along the sample edge, *i.e.* along x or y), in the case of wurtzite material with (0 0 0 1) orientation. An additional E_1(LO) phonon mode is seen in $y(zy)x$ configuration. The observed phonon lines in the crystallites spectra acquired with an excitation orthogonal to the sample surface (*i.e.* along *z*) are thus a clear indication of their non-polar or semi-polar orientation. A similar approach has been successfully used for the Raman analysis of polycrystalline AlN films grown by HTCVD [30] and AlN fibers grown by sublimation growth [39]. The E_2(h) and A_1(LO) phonon modes, characteristic of (0 0 0 1) planes have been observed in the smooth surface (A) of Fig. 7(a) and the appearance of E_1(TO) and E_1(LO), as well as the disappearance of the A_1(LO) mode, is the signature of $(10\bar{1}1)$ facets observed in disoriented crystallites (B) of Fig. 7(a) [40].

Fig. 7(b–c) shows the cross sectional and surface FE-SEM images of a HT-AlN sample with 750 °C NL. The disoriented crystallites and c-axis oriented area have been explicitly examined in the SEM images. This mixed (*c*-axis oriented and dis-oriented crystallites) AlN growth has been observed on HT-AlN samples grown with 650, 750 and 850 °C NLs, but it is more pronounced at lower temperature NLs. The disoriented crystallites have been predominant when the thickness is above 0.5 μm for all the HT-AlN layers grown with 650 °C NLs. High density of NIs, too low thickness of NLs, and HT-AlN growth occurring on tilted NIs result in the formation of polycrystalline samples. On the other hand, for HT-AlN layers with NLs deposited at 750 and 850 °C, the disoriented crystallites formation is annihilated and the growth along c-axis is favoured. A higher growth temperature for NLs is found to promote the formation of c-oriented AlN layers without disoriented crystallite.

Improvement in structural quality, surface morphology and epitaxial growth along *c*-axis has been obtained when increasing the NLs deposition temperature from 650 to 850 °C. The lowest (0 0 0 2) FWHM value of 1900 arcsec has been obtained for HT-AlN samples grown at 1200 °C on NLs grown at 850 °C. Nevertheless the use of NLs for HT-AlN growth provides stabilization of epitaxial growth compared to direct growth (without NLs) of HT-AlN films at 1200 °C, which always result in the growth of completely polycrystalline AlN films for the same operating conditions. These results show the significance of NLs on improving epitaxial growth and crystalline quality. In order to improve the crystalline quality of the HT-AlN layers, a higher growth temperature has been investigated.

3.2.4. *Characterizations of HT-AlN layers grown at 1400 °C with NLs*

A HT-AlN layer grown at 1400 °C on a NL deposited at 850 °C has been studied. The recrystallization and HT-AlN deposition have been performed at 1400 °C using the same precursors flow and V/III ratio as used for AlN layers grown at 1200 °C. $\theta - 2\theta$ scan, XRC, Raman and FE-SEM analysis have been performed on this sample.

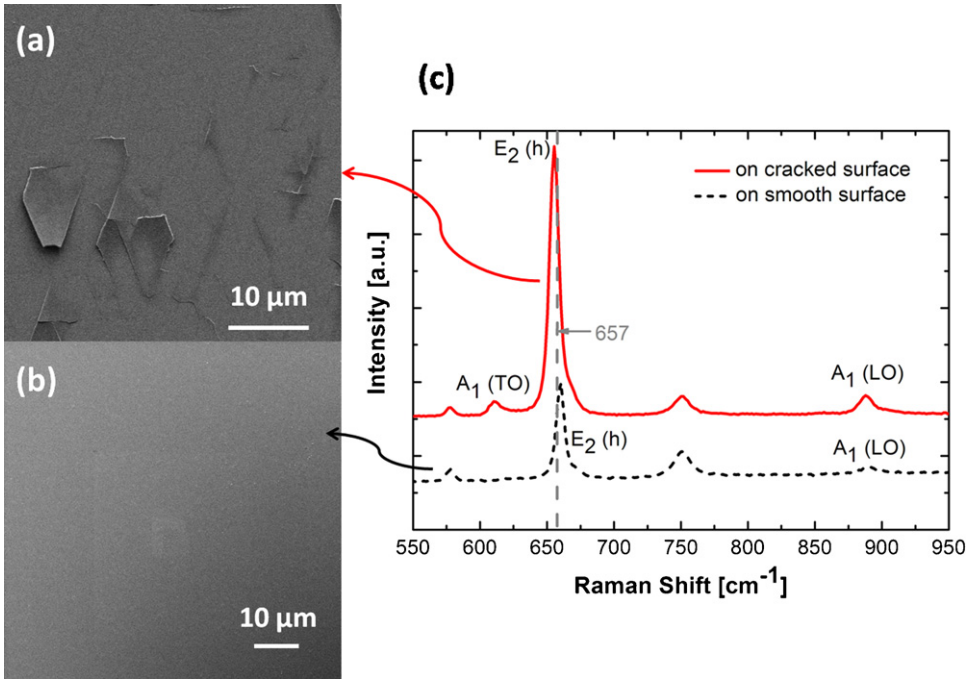

Fig. 8. Scanning electron microscopy images of (a) cracked surface, (b) smooth surface and (c) corresponding Raman spectra (HT-AlN layer grown at 1400 °C). E_2(h) phonon wave number at 657 cm^{-1} for stress-free AlN is also indicated.

Only (000ℓ) peaks have been found from XRD on $\theta - 2\theta$ scan (not shown). Two kinds of surfaces such as cracked or peeled off surface (Fig. 8a) and smooth or specular surface (Fig. 8b) have been observed from the HT-AlN sample.

A non-uniformity of thickness from 1 to 2 μm throughout the 2″ wafer has been observed from cross sectional SEM images. The smooth surface corresponds to an AlN layer thickness of about 1 μm whereas the cracked layer with high strain exhibits a thickness between 1.5 and 2 μm. It might be due to a non-homogeneous gas flow inside the HVPE reactor. It seems that higher AlN thickness leads to more strain inside the AlN layer. This cracking phenomenon might be also attributed to the difference between the thermal expansion coefficient of sapphire and AlN. It could happen during the cooling down.

Fig. 8(c) shows the Raman spectra observed on the two kinds of surfaces, specular and cracked. In Fig. 8(c) the decrease in the E_2(h) phonon frequency to 655 cm^{-1} for the cracked surface exhibits an in-plane tensile stress. On the other hand, the increase in the E_2(h) phonon frequency to 660 cm^{-1} shows that AlN epilayers with smooth surface are in a compressive strain state. The change from tensile to compressive strain is the result of the AlN layer pealing from the cracked part of the sample. The bending of the AlN surface is thus due to the strain relaxation (from compressive to relaxed or even tensile) when the AlN is no longer strained on Al_2O_3. XRC for the (0 0 0 2) AlN peak has been performed. The FWHM of HT-AlN layer has been obtained as 860 arcsec in the smooth area and the corresponding screw dislocation density is about 2×10^9 cm^{-2}. XRC analysis show the improved quality of HT-AlN layers grown at 1400 °C instead of 1200 °C. RMS roughness value of 5.6 nm (scan 5 μm × 5 μm) also indicates a smoother surface morphology compared to HT-AlN layers grown at 1200 °C. Further investigations on the NLs temperatures, precursor flows and growth temperature of HT-AlN layers will have to be done in order to increase and optimize the quality of AlN epilayers using NLs.

4. Conclusions

Growth of HT-AlN layers with nucleation layers have been performed using HT-HVPE at 1200 and 1400 °C. The influences of growth temperature and HT-treatment on nucleation layer morphology and thickness have been studied. It has been concluded that the existence of NLs desorption at 1200 °C and rearrangement of the NL surface during high temperature treatment. Improvement in structural quality, surface morphology and epitaxial growth along c-axis has been observed when increasing the NLs deposition temperature from 650 to 850 °C. Nucleation layers grown at 650 °C favour the growth of polycrystalline AlN with a semi-polar ($10\bar{1}1$) preferred orientation whereas nucleation layers deposited at 750 and 850 °C assist to grow (0 0 0 2) AlN epilayers at 1200 °C. The structural quality and surface morphology have been improved with increasing growth temperature of the HT-AlN layers from 1200 to 1400 °C. Further improvements in AlN epilayer quality and realizing crack free surface morphology is found to require better control of the NL deposition step and optimization of high temperature growth steps to enhance the coalescence and to obtain low density of nucleation islands.

Acknowledgements

The authors would like to thank Grégory Berthomé from SIMaP for extending AFM characterization facility, Rachel Martin from CMTC for FE-SEM observations, Denis Sauvage and Seddik Benmamar from ACERDE for help and support in CVD instrumentation. This work has been supported by ACERDE and by the French ANR research program DUVED-P-NANO Contract Nb. ANR-08-NANO-007 in the field of AlN epitaxial growth for the development of deep UV LEDs. Manavaimaran Balaji gratefully acknowledges European Commission Erasmus Mundus External Window Lot (13) – India4EU programme and AICTE-NDF for the financial support.

References

[1] A. Khan, K. BalaKrishnan, T. Katona, Nat. Photon. 2 (2008) 77.
[2] M.B. Assouar, O. Elmazria, P. Kirsch, P. Alnot, V. Mortet, C. Tiusan, J. Appl. Phys. 101 (2007) 114507.
[3] U.K. Mishra, P. Parikh, Y.F. Wu, Proc. IEEE 90 (2002) 1022.
[4] M.A. Mastro, D. Tsvetkov, V. Soukhoveev, A. Usikov, V. Dmitriev, B. Luo, F. Ren, K.H. Baik, S.J. Pearton, Solid-State Electronics 47 (2003) 1075.
[5] H. Morkoc, S. Strite, G.B. Gao, M.E. Lin, B. Sverdlov, M. Burns, J. Appl. Phys. 76 (1994) 1363.
[6] L. Liu, J.H. Edgar, Mater. Sci. Eng. R 37 (2002) 61.
[7] L.J. Schowalter, G.A. Slack, J.B. Whitlock, K. Morgan, S.B. Schujman, B. Raghothamachar, M. Dudley, K.R. Evans, Phys. Status Solidi C 0 (2003) 1997.
[8] R. Schlesser, R. Dalmau, Z. Sitar, J. Cryst. Growth 241 (2002) 416.
[9] M. Boćkowski, M. Wróblewski, B. Łucznik, I. Grzegory, Mater. Sci. Semicond. Proc. 4 (2001) 543.
[10] H. Isobe, F. Kawamura, M. Kawahara, M. Yoshimura, Y. Mori, T. Sasaki, Jpn. J. Appl. Phys. 44 (2005) L488.
[11] S. Yoshida, M. Misawa, Y. Fujii, S. Takeda, H. Hayakawa, S. Gonda, A. Iton, J. Vac. Sci. Technol. 16 (1979) 990.
[12] M. Imura, K. Nakano, N. Fujimoto, N. Okada, K. Balakrishnan, M. Iwaya, S. Kamiyama, H. Amano, I. Akasaki, T. Noro, T. Takagi, A. Bandoh, Jpn. J. Appl. Phys. 45 (2006) 8639.
[13] Y. Kumagai, T. Yamane, T. Miyaji, H. Murakami, Y. Kangawa, A. Koukitu, Phys. Status Solidi C 0 (2003) 2498.
[14] A. Claudel, E. Blanquet, D. Chaussende, M. Audier, D. Pique, M. Pons, J. Cryst. Growth 311 (2009) 3371.
[15] D.F. Bliss, V.L. Tassev, D. Weyburne, J.S. Bailey, J. Cryst. Growth 250 (2003) 1.
[16] R. Fan, H. Zhi-Biao, H. Jian-Nan, Z. Chen, L. Yi, Chin. Phys. B 19 (2010) 116801.
[17] Y. Kumagai, T. Yamane, A. Koukitu, J. Cryst. Growth 281 (2005) 62.
[18] K. Akiyama, T. Araki, H. Murakami, Y. Kumagai, A. Koukitu, Phys. Status Solidi C 4 (2007) 2297.
[19] Y. Kumagai, K. Akiyama, R. Togashi, H. Murakami, M. Takeuchi, T. Kinoshita, K. Takada, Y. Aoyagi, A. Koukitu, J. Cryst. Growth 305 (2007) 366.
[20] J. Tajima, Y. Kubota, R. Togashi, H. Murakami, Y. Kumagai, A. Koukitu, Phys. Status Solidi C 5 (2008) 1515.
[21] A. Dadgar, A. Krost, J. Christen, B. Bastek, F. Bertram, A. Krtschil, T. Hempel, J. Blasing, U. Haboeck, A. Hoffmann, J. Cryst. Growth 297 (2006) 306.
[22] N. Okada, N. Kato, S. Sato, T. Sumii, T. Nagai, N. Fujimoto, K. Balakrishnan, M. Iwaya, S. Kamiyama, H. Amano, M. Imura, I. Akasaki, H. Maruyama, T. Takagi, T. Noro, A. Bandoh, J. Cryst. Growth 298 (2007) 349.
[23] J.N. Kuznia, M. Asif Khan, D.T. Olson, Ray Kaplan, Jamie Freitas, J. Appl. Phys. 73 (1993) 4700.
[24] X.H. Wu, D. Kapolnek, E.J. Tarsa, B. Heying, S. Keller, B.P. Keller, U.K. Mishra, S.P. DenBaars, J.S. Speck, Appl. Phys. Lett. 68 (1996) 1371.
[25] M. Balaji, A. Claudel, V. Fellmann, I. Gélard, E. Blanquet, R. Boichot, S. Coindeau, H. Roussel, D. Pique, K. Baskar, M. Pons, Phys. Status Solidi C, doi:10.1002/pssc.201100357.
[26] Y. Kumagai, T. Yamane, T. Miyaji, H. Murakami, Y. Kangawa, A. Koukitu, Phys. Status Solidi C (2003) 2498.
[27] K. Lorenz, M. Gonsalves, Wook Kim, V. Narayanan, S. Mahajan, Appl. Phys. Lett. 77 (2000) 3391.
[28] T. Lang, M. Odnoblyudov, V. Bougrov, S. Suihkonen, M. Sopanen, H. Lipsanen, J. Cryst. Growth 292 (2006) 26.
[29] D.G. Zhao, J.J. Zhu, Z.S. Liu, S.M. Zhang, Hui Yang, D.S. Jiang, Appl. Phys. Lett. 85 (2004) 1499.
[30] A. Claudel, E. Blanquet, D. Chaussende, R. Boichot, R. Martin, H. Mank, A. Crisci, B. Doisneau, P. Chaudouet, S. Coindeau, D. Pique, M. Pons, J. Electrochem. Soc. 158 (3) (2011) H328.
[31] Y. Taniyasu, M. Kasu, T. Makimoto, J. Cryst. Growth 298 (2006) 310.
[32] T. Onuma, T. Shibata, K. Kosaka, K. Asai, S. Sumiya, M. Tanaka, T. Sota, A. Uedono, S.F. Chichibu, J. Appl. Phys. 105 (2003) 023529.
[33] K.-i. Eriguchi, T. Hiratsuka, H. Murakami, Y. Kumagai, A. Koukitu, J. Cryst. Growth 310 (2008) 4016–4019.
[34] T. Koyama, M. Sugawara, T. Hoshi, A. Uedono, J.F. Kaeding, R. Sharma, S. Nakamura, S.F. Chichibu, Appl. Phys. Lett. 90 (2007) 241914.
[35] A. Uedono, S. Ishibashi, S. Keller, C. Moe, P. Cantu, T.M. Katona, D.S. Kamber, Y. Wu, E. Letts, S.A. Newman, S. Nakamura, J.S. Speck, U.K. Mishra, S.P. DenBaars, T. Onuma, S.F. Chichibu, J. Appl. Phys. 105 (2009) 054501.
[36] V.Y.U. Davydov, Yu E. Kitaev, I.N. Goncharuk, A.N. Smirnov, J. Graul, O. Semchinova, D. Uffmann, M.B. Smirnov, A.P. Mirgorodsky, R.A. Evarestov, Phys. Rev. B 58 (1998) 12899.
[37] C.A. Arguello, D.L. Rousseau, S.P.S. Porto, Phys. Rev. 181 (1969) 135.
[38] M. Kuball, Surf. Interface Anal. 31 (2001) 987.
[39] H.Q. Bao, X.L. Chen, H. Li, G. Wang, B. Song, W.J. Wang, Appl. Phys. A 94 (2009) 173.
[40] M. Bickermann, B.M. Epelbaum, P. Heimann, Z.G. Herro, A. Winnacker, Appl. Phys. Lett. 86 (2005) 131904.